Desalination and Water Treatment
www.deswater.com

doi: 10.1080/19443994.2015.1112841

57 (2016) 20837–20855
September

Taylor & Francis
Taylor & Francis Group

Poly(acrylic acid)-zeolite nanocomposites for dye removal from single and binary systems

Arash Almasian[a], Mazeyar Parvinzadeh Gashti[b,*], Mohammad Ebrahim Olya[a], Ghazaleh Chizari Fard[c]

[a]*Department of Environmental Research, Institute for Color Science and Technology, Tehran, Iran, emails: almasian-ar@icrc.ac.ir (A. Almasian), olya-me@icrc.ac.ir (M.E. Olya)*
[b]*Young Researchers and Elites Club, Yadegar-e-Imam Khomeini (RAH) Branch, Islamic Azad University, P.O. Box 18155/144, Tehran, Iran, email: mparvinzadeh@gmail.com*
[c]*Department of Textile, Yazd Branch, Islamic Azad University, Yazd, Iran, email: chizarifard@iauyazd.ac.ir*

Received 16 June 2015; Accepted 18 October 2015

ABSTRACT

In this research, nanocomposites of zeolite/acrylic acid were synthesized with different amount of acrylic acid (AA) as monomer and ammonium persulfate (APS) as an initiator to remove cationic dyes from wastewater in single and binary systems. Basic Red 46 (BR46) and Basic blue 41 (BB41) were used as the cationic dyes. The surface characteristics of nanocomposites were investigated using Fourier transform infrared spectra (FTIR) and scanning electron microscope. FTIR results confirmed successful attachment of acrylic acid on the zeolite surface. The influence of different factors such as initial monomer concentration and amount of initiator on dye removal in single system, and adsorbent dosage, pH, and initial dye concentration in single and binary systems were evaluated. The dye adsorption isotherm and kinetics were studied. Results indicated that adsorption of BR46 and BB41 onto nanocomposites is well fitted with Langmuir isotherm and the rate of sorption was found to conform to pseudo-second-order kinetic with good correlation. The maximum dye adsorption capacity (Q_0) of composites for two different amounts of AA and APS in nanocomposite (0.17 mmol AA + 3.50 mmol APS and 0.26 mmol AA + 6.57 mmol APS) was 2,439.02 and 2,702.70 for BB41, 2,272.72 and 2,380.95 mg/g for BR46 in single system, 2,083.33 and 2,127.65 for BB41, 1,785.71 and 1,923.07 mg/g for BR46 in binary system. Results illustrated that zeolite/acrylic acid nanocomposites could be suggested as an efficient nanoadsorbent to remove cationic dyes from wastewaters.

Keywords: Composite materials; Chemical synthesis; Fourier transform infrared spectroscopy (FTIR); Adsorption

1. Introduction

With the growing use of a variety of dyes, the pollution from dye wastewater is becoming a major environmental problem. It is known that there are about 3,000 types of dyes in the world market [1]. Among them, synthetic dyes having potential toxicity and low biodegradability. In this regard, some water-soluble cationic dyes could particularly cause great damage to natural ecosystems when they are

*Corresponding author.

1944-3994/1944-3986 © 2015 Balaban Desalination Publications. All rights reserved.

discharged with wastewater [2]. Although some treatment methods for removal of these dyes have been developed, economic, and effective processing still remains a significant issue. The methods of dye removal from industrial wastewaters contain many processes such as biological treatment, coagulation, flotation, electrochemical techniques, adsorption, and oxidation [3–8]. Among them, adsorption is considered to be relatively superior to other techniques because of low cost, simplicity of design, availability, and ability to treat dyes in more concentrated form [9,10].

In general, absorbents can be divided into four categories including natural absorbents, biomass, activated carbon and synthetic polymers [11–15]. A natural absorbent fit economically, but requires chemical modification. Salleh et al. used agricultural solid wastes for cationic and anionic dye adsorption [16]. Biomass absorbent do not have toxic effect on microorganisms and have a good performance, but the process is slow. Gao et al. removed heavy metals from aqueous solutions by biochars derived from anaerobically digested biomass [17]. Activated carbon is the most attractive absorbent with high absorption capacity, but is inactive against dyes and expensive. In this regard, Bouhamed et al. used active carbon for multicomponent adsorption of copper, nickel, and zinc from aqueous solutions [18]. Polymer absorbent are growing as an alternative in synthesis of absorbents due to their high surface area, high mechanical strength, and adjustable pore size distribution. In this subject, Khairkar et al. produced chitosan-g-poly (acrylic acid-co-acrylamide) composites for the removal of heavy metals [19].

One of the minerals which are previously considered as an adsorbent is zeolite. This microporous commercial mineral is composed of crystalline aluminosilicates with three-dimensional structure. The framework of SiO_4 and AlO_4 tetrahedral are linked together by shared oxygen atoms to form the final compound [20,21]. Sodalite as the simplest structure of tetrahedral units is obtained by octagon plates. The type of zeolite 4A is more recognized as it has more open structure than sodilate (Fig. 1) [22,23]. The negative charge of zeolite 4A framework is neutralized by Na^+ and it has been utilized for adsorption of cationic compounds [24].

Monomers can be polymerized onto different inorganic particles to increase the adsorption capacity and removal of pollutants [25]. It was previously shown that poly (acrylic acid) as a super-absorbent polymer can effectively absorb large amounts of dyes [26–28]. Moreover, kaolin/poly acrylic acid composites were demonstrated for removal of dyes from wastewaters

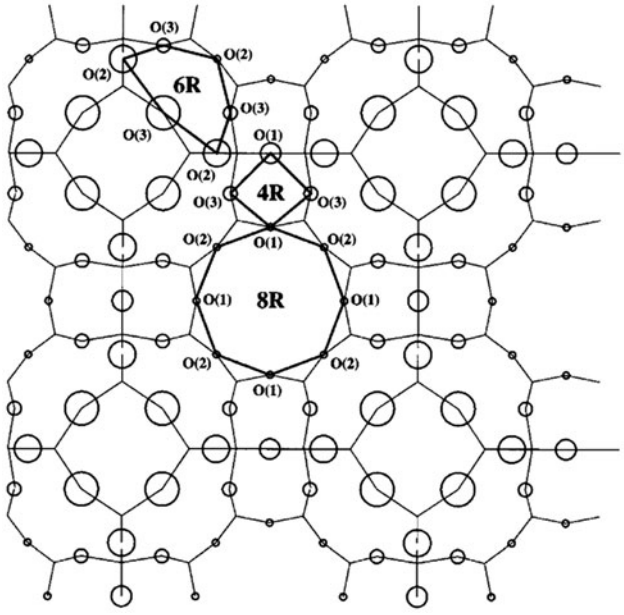

Fig. 1. Schematic diagram of the zeolite 4A crystal. Only the oxygen atoms are shown and are represented by circles, with the size of circle indicating depth. Examples of an oxygen eight-, six-, and four-ring are illustrated by bold lines and labeled 8R, 6R, and 4R, respectively. The oxygen atoms are labeled O(1), (2), and O(3) according to convention [12].

[29]. Another study for the removal of Basic Fuch dye by laponite/poly acrylamide nanocomposite has been performed [30]. It is stated that methyl violet as a cationic dye can be removed from aqueous solutions by ternary nanocomposites of attapulgite/polyacrylic acid/poly (acrylamide) [31].

However, to the best of the authors' knowledge, zeolite/acrylic acid nanocomposite has not yet been synthesized for removal of cationic dyes from single and binary systems. We used zeolite as an inorganic substrate and acrylic acid as an absorbent monomer for producing a nanoadsorbent. This is due to its superior absorption properties in comparison with many other inorganic particles, monomers, and nanocomposites. Also, the influence of several parameters such as adsorbent amount, dye concentration, and pH on the adsorption capacity was evaluated. The equilibrium data have also been analyzed using various adsorption isotherms.

2. Experimental work

2.1. Materials

Zeolite 4A (LTA, free diameter: 8-ring: 0.41 nm, Si/Al ratio: ~1, Pores/ Channels: 3D Spherical

1.14 nm cavities) with chemical formula of $Na_{12}Al_{12}Si_{12}O_{48}$ supplied by *Paksan* Co. (Iran). Cetyltrimethyl ammonium bromide ($C_{16}H_{33}N^+$ $(CH_3)_3Br^-$, CTAB), acrylic acid (AA), ammonium persulfate (APS), and sodium chloride (NaCl) were supplied by Merck Chemical Co., Germany.

Basic Red 46 and Basic blue 41 as cationic dyes were purchased from *AlvanSabet* Co. (Iran), and were used without purification. The molecular structure of the dyes is shown in Fig. 2.

2.2. Synthesis of zeolite–acrylic acid nanocomposites

Preparation of zeolite–acrylic acid nanocomposites was performed by a two-step method. First, 2 g of zeolite was dispersed in distilled water with 10% (o.w.f) CTAB (70%) and 10% (o.w.f) NaCl and stirred for 3 h at 80˚C, then centrifuged and washed by successive agitations/centrifugation with distilled water for several times. The wet paste was fully dried at 50˚C [32–34]. Second, various amounts of AA (0.17 and 0.26 mmol) and APS (3.50 and 6.57 mmol) were added to the zeolite with different stirring time (3 and 4 h) at 70˚C. Finally, all the samples were centrifuged and washed by successive agitations/centrifugation with distilled water and dried at 60˚C.

2.3. Characterizations

The chemical specifications of produced composites were examined by the Fourier transform infrared (FTIR) spectroscopy (ThermoNicolet NEXUS 870 FTIR (Nicolet Instrument Corp., USA)). The surface morphology of nanocomposites was investigated using a scanning electron microscope (SEM, LEO1455VP, ENGLAND). Furthermore, nanocomposites were also determined by energy dispersive X-ray microanalysis (EDX) attached to the SEM. The released acrylic acid from nanocomposites was tested by a TOC analyzer (TOC-L shimadzu). The thermogravimetric analysis (TGA) was performed on a Perkin Elmer thermoanalyzer (Pyris diamond SII). In each case, a 5 mg sample was examined under a N_2 at a heating rate of 5˚C/min from 50 to 600˚C. Surface chemical characterization was performed by X-ray photoelectron spectroscopy (XPS) using a Thermo ESCALAB 280 system with Al/Kα (hv = 1,486.6 eV) anode mono X-ray source. The grafting yield was determined as follows:

$$\text{Grafting yield } (\%) = \frac{W_g - W_0}{W_0} \times 100 \quad (1)$$

where W_g and W_0 are the weight of zeolite before and after the grafting process, respectively.

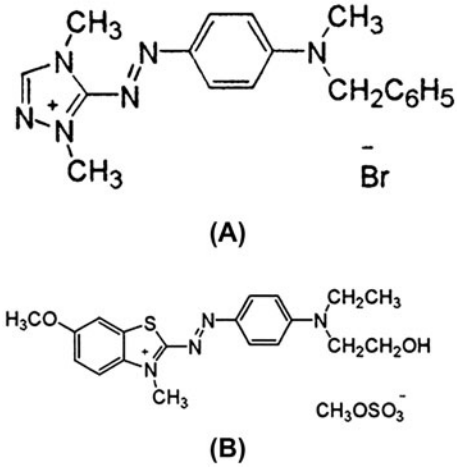

Fig. 2. Chemical structure of (A) Basic Red 46 (BR46) with 401.3 molecular weight and (B) Basic Red 41 (BB41) with 296.37 molecular weight.

2.4. Batch adsorption and decolorization experiments

BR46 and BB41 were selected as pollutants to evaluate the adsorption capacity of the zeolite–acrylic acid nanocomposites. The maximum wavelength (λ_{max}) used for determination of the residual concentration of BR46 and BB41 in the supernatant solution using UV–vis spectrophotometry (CECIL 2021) were 530 and 590 nm, respectively.

The adsorption measurements were conducted by mixing the nanocomposites in a batch containing 200 mL of a dye solution (40 mg/L) at pH of 6.8.

The effect of adsorbent dosage on dye removal in single and binary systems was investigated by contacting 200 mL of dye solution (40 mg/L) at room temperature and pH 6.8 for 60 min. Different amounts of adsorbent (8×10^{-4}–7×10^{-3} g) were applied.

The effect of pH on dye removal in single and binary systems was conducted by adding 0.004 g adsorbent, and 200 mL of dye solution (40 mg/L) at different pH values (3.1, 6.8, and 9.1). The pH of each solution was adjusted to a desired value using HCl or NaOH solution.

The effect of initial dye concentration on the dye removal in single system was studied by adding 0.004 g of adsorbent to different dye concentrations (40, 60, 80, and 100 mg/L) at pH 6.8, and 200 mL of dye solution. For a binary system, components A and

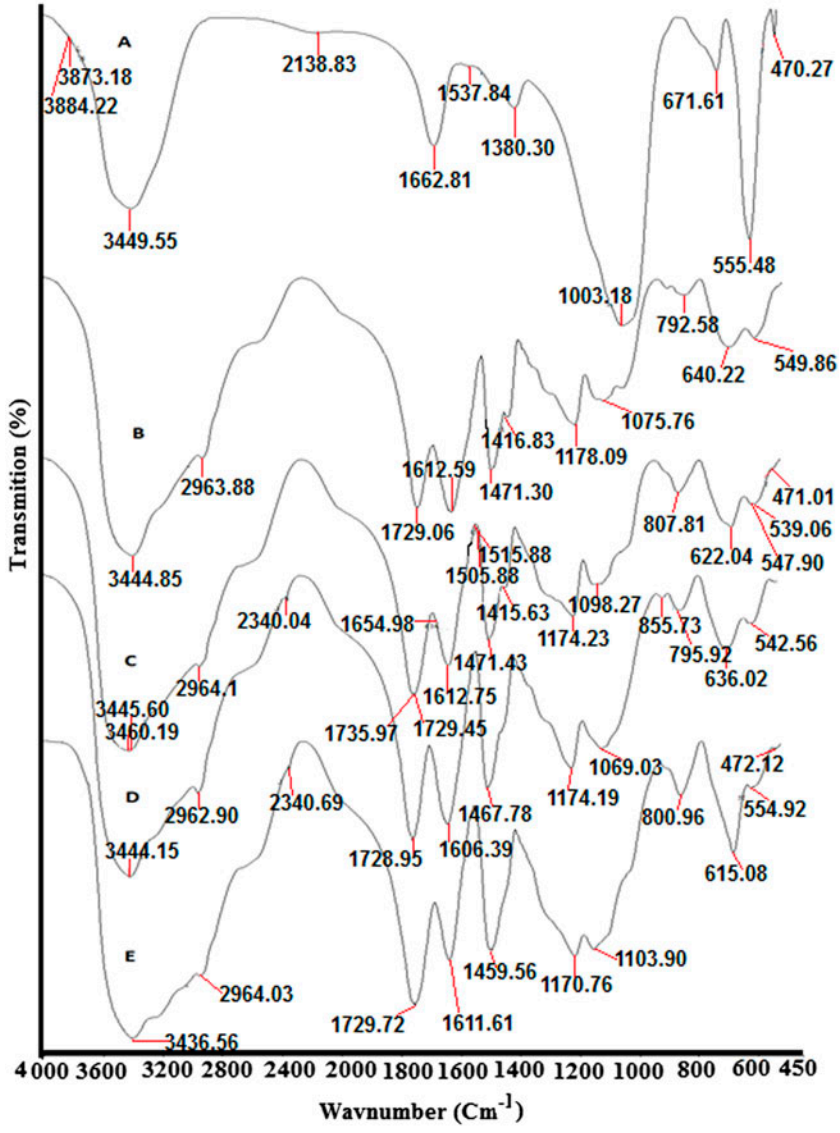

Fig. 3. FTIR spectra of the (A) untreated zeolite, (B) zeolite treated with 0.17 mmol AA and 3.50 mmol APS for 3 h, (C) zeolite treated with 0.17 mmol AA and 3.50 mmol APS for 4 h, (D) zeolite treated with 0.26 mmol AA and 6.57 mmol APS for 3 h, and (E) zeolite treated with 0.26 mmol AA and 6.57 mmol for 4 h.

B were measured at λ_1 and λ_2, respectively, to give optical densities of d_1 and d_2 [31]:

$$C_A = \frac{K_{B2}d_1 - K_{B1}d_2}{K_{A1}K_{B2} - K_{A2}K_{B2}} \quad (2)$$

$$C_B = \frac{K_{A1}d_2 - K_{A2}d_1}{K_{A1}K_{B2} - K_{A2}K_{B2}} \quad (3)$$

where K_{A1}, K_{B1}, K_{A2}, and K_{B2} are the calibration constants for components A and B at the two wavelengths λ_1 and λ_2, respectively.

The amounts of decolorization were determined as a function of time according to the following equation:

$$\text{Dec } \% = \frac{A_0 - A}{A_0} \times 100 \quad (4)$$

where A_0 and A are dye concentration at $t = 0$, t.

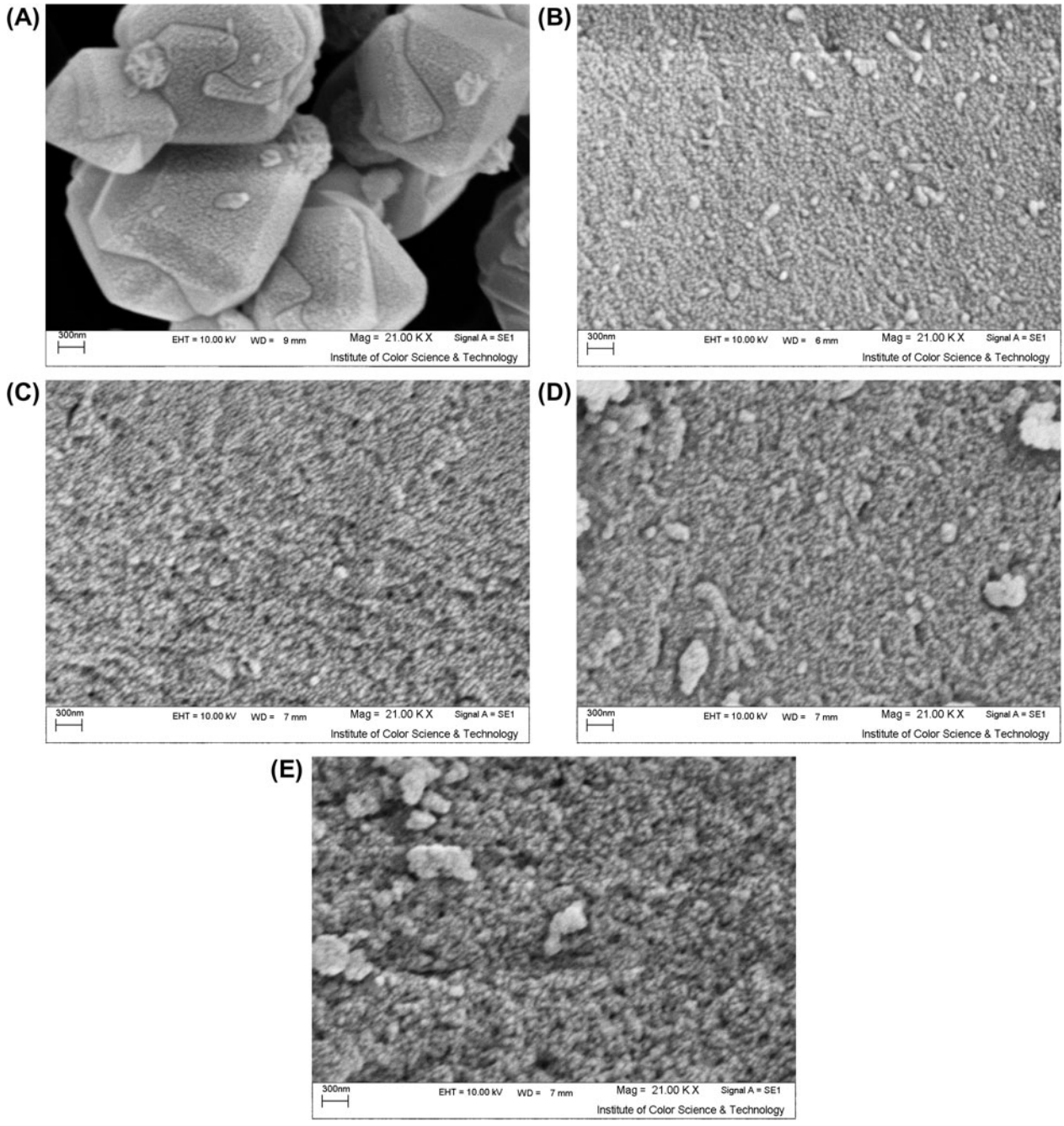

Fig. 4. SEM images (A) untreated zeolite, (B) zeolite treated with 0.17 mmol AA and 3.50 mmol APS for 3 h, (C) zeolite treated with 0.26 mmol AA and 6.57 mmol APS for 3 h, (D) zeolite treated with 0.17 mmol AA and 3.50 mmol APS for4 h, and (E) zeolite treated with 0.26 mmol AA and 6.57 mmol APS for 4 h.

3. Results and discussions

3.1. Chemical characterization of nanocomposites by FTIR spectra

In order to investigate the chemical properties of nanocomposites, the FTIR spectra of untreated zeolite and various nanocomposites (B–E) are shown in Fig. 3. FTIR spectrum of untreated zeolite showed a broad peak at 3,449.5 cm^{-1} corresponding to stretching vibration of surface hydroxyl groups. The peaks appeared at 1,662.81, 1,003.18, 671.61, and 555.48 cm^{-1} correspond to the H–O–H bending vibration of free or

Table 1
TOC values

Sample	Distilled water	Zeolite (0.17 mmol AA + 3.50 mmol APS, 4 h)	Zeolite (0.26 mmol AA + 6.57 mmol, 4 h)
TOC value	0.010	0.009	0.011

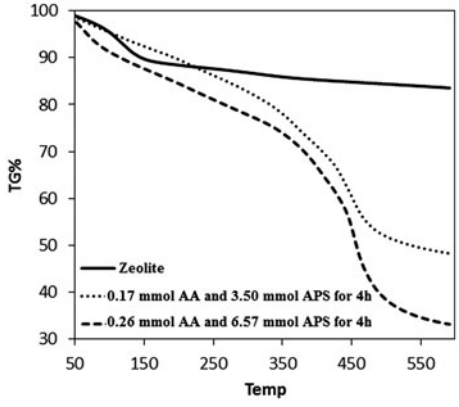

Fig. 5. TGA curves of zeolite together with produced nanocomposites.

absorbed water, stretching vibration Si–O–Al band [35], symmetric stretch of Si–O–Si bond [36], and bending vibrations of Si–O [37], respectively. The OH stretching band appeared in the region between 3,100 and 3,500 cm^{-1} for all nanocomposites. In the spectra of nanocomposites, the exhibition of peaks at 2,964, 1,471.43, 1,415.63, 807.81, and 622.04 cm^{-1} attributed to the CH_2 bending vibrations, CH_3 bending vibrations, CH out of plane bending and CH out of plane deformation of composites, respectively [38]. The C=O stretching vibrations appeared at 1,729 cm^{-1} is assigned to COOH groups in the composites [39] confirming successful attachment of acrylic acid on the zeolite surface.

3.2. SEM analysis

SEM is one of the best methods to study the morphology and appearance of adsorbents. This instrument is useful for determining the particle shape and size distribution as well as porosity. Fig. 4 showed SEM images of untreated zeolite and various zeolite–acrylic acid nanocomposites. The porosity of untreated zeolite has a size of approximately 0.4–0.7 nm [40] so, acrylic acid monomer cannot polymerize into the zeolite pores perforce, and it was formed on the zeolite surface. As can be seen from images, porous network was further developed in prepared nanocomposites.

3.3. Evaluation of nanocomposites by TOC, TGA, and mapping

In order to evaluate the structure of nanocomposites and possibility of acrylic acid releasing, TOC, TGA, and Map analyses were performed and results are shown in Table 1 and Figs. 5 and 6, respectively.

As can be seen from Table 1, TOC values for distilled water and nanocomposites after immersion in distilled water are close together. TOC result proved that acrylic acid was not released from nanocomposites. Fig. 5 showed the TG thermogram of produced nanocomposite samples. As can be seen, zeolite showed a two-stage weight loss. The first stage occurred at around 160˚C and, the weight loss was about 19%. This weight loss is due to the physical water loss. The second stage is around 220˚C with the weight loss of 5%. Evaporation of the chemically absorbed water can be the reason of weight loss at second stage [41].

According to Fig. 5, zeolite–acrylic acid nanocomposites showed a three-stage weight loss in the range of 170–650˚C. The weight loss in the first stage is about 7% before 170˚C due to evaporation of physical absorbed water. Moreover, the samples have experienced two major weight-loss stages with distinct separation. The results showed that the main thermal decomposition process is in the range of 230–470˚C, resulting from the chain scission of macromolecular framework and the formation of stable intermediates. Third stage starts at around 550˚C, involving decomposition of the carbonized products. With the addition of polymer, the decomposition became harder due to the increase in the activation energy required for thermal degradation [42]. The three-stage decomposition features for the zeolite (0.17 mmol AA + 3.50 mmol APS, 4 h) and zeolite (0.26 mmol AA + 6.57 mmol, 4 h) are identical. For zeolite (0.26 mmol AA + 6.57 mmol, 4 h), the amount of weight loss is lower until 210˚C probably due to existence of more hydrophilic group that can absorb water. Moreover, the weight loss increased after 210˚C. This is due to degradation of the higher amount of polymer in the zeolite (0.26 mmol AA + 6.57 mmol, 4 h) sample. From TGA analysis, generation of zeolite–acrylic acid nanocomposites is confirmed.

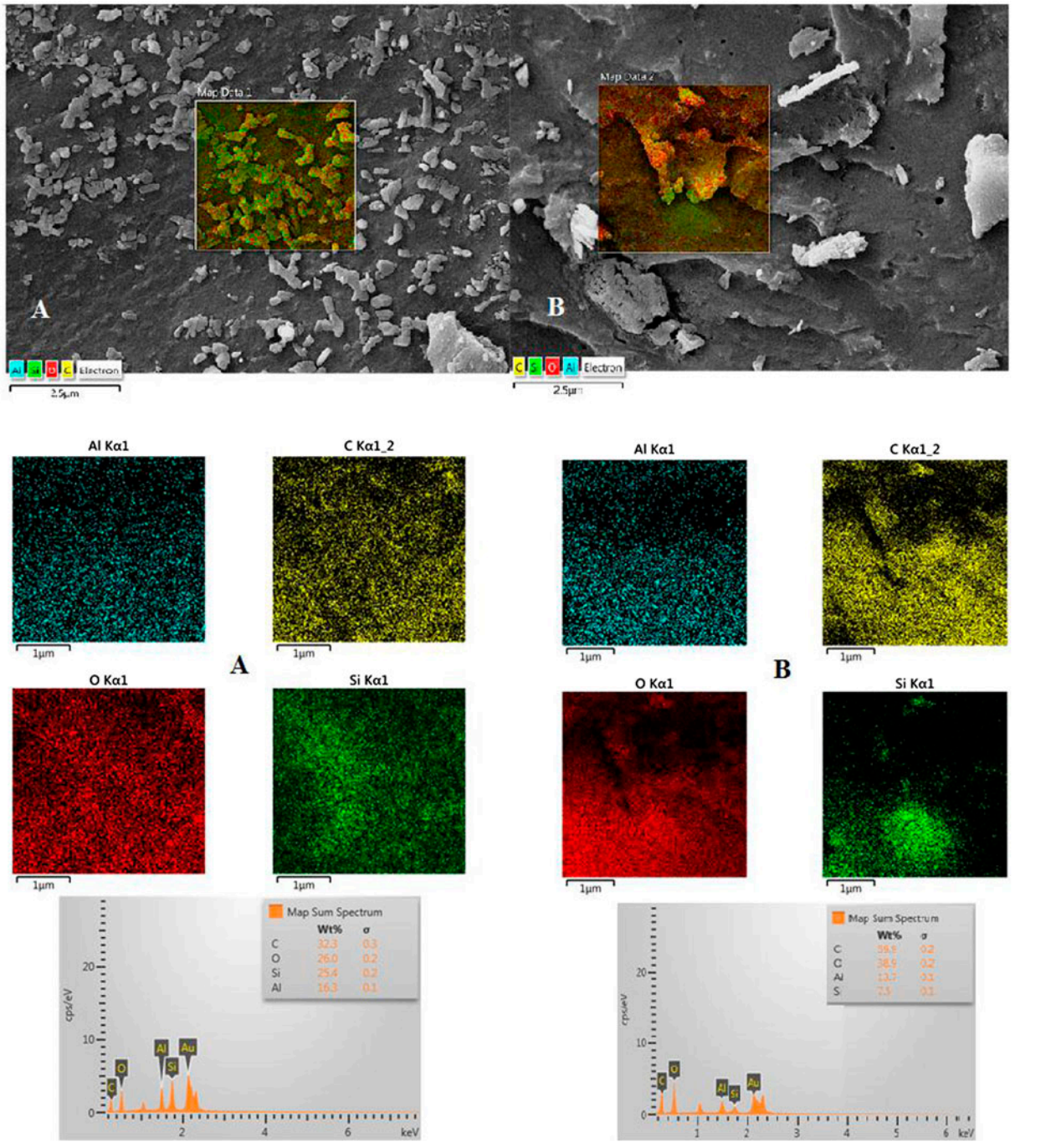

Fig. 6. Map and EDX images (A) zeolite treated with 0.17 mmol AA and 3.50 mmol APS for4 h and (B) zeolite treated with 0.26 mmol AA and 6.57 mmol APS for 4 h.

Fig. 6 represented the MAP images from nanocomposites. It is obvious that carbon element related to acrylic acid is well dispersed on the zeolite surface. Distribution of Si and Al attributed to zeolite which is homogenous. Also, EDAX analysis showed the presence of carbon on zeolite surface which is increased with an increase in acrylic acid in nanocomposites. A homogenous distribution of elements in produced nanocomposites proves successful synthesizing of zeolite–acrylic acid nanocomposites.

Table 2
XPS analysis and gravimetry method of different synthesized nanocomposites

Analysis	Element	Zeolite	Zeolite (0.17 mmol AA + 3.50 mmol APS, 4 h)	Zeolite (0.26 mmol AA + 6.57 mmol, 4 h)
XPS	Oxygen (O)	43.3%	51.1%	55.4%
	Carbon (C)	0	20.3%	27.2%
Gravimetry	Weight	2.0 g	2.98 g	3.45 g

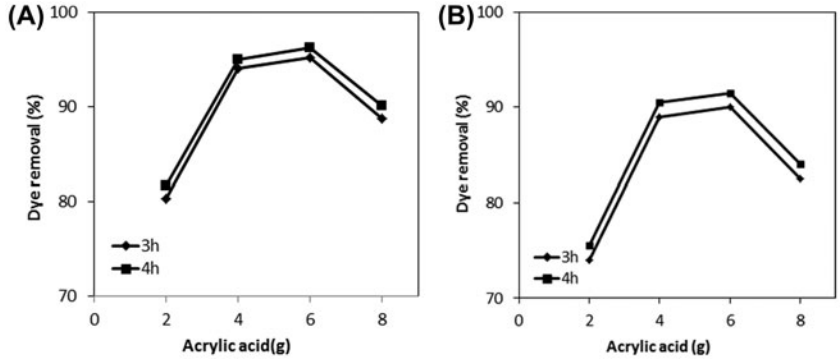

Fig. 7. Effect of the initial AA concentration on dye adsorption properties of nanocomposite produced by 3.50 mmol initiator and 2 gr zeolite, (A) BB41 and (B) BR46.

3.4. Optimization of grafting conditions

XPS result showed that the amount of carbon and oxygen increased after the grafting of acrylic acid on the surface of zeolite (Table 2). Also, gravimetry analysis showed that the weight of zeolite increased about 32.8 and 42.1% for zeolite (0.17 mmol AA + 3.50 mmol APS,4 h) and zeolite (0.26 mmol AA + 6.57 mmol, 4 h), respectively.

3.5. Effect of initial monomer concentration

The effect of initial AA concentration on removal of BR46 and BB41 in single system is shown in Fig. 7. The dye adsorbency is increased with the increase in AA concentration. It can be stated that the number of adsorption sites increases with increasing the amount of acrylic acid to 0.26 mmol. However, results showed that the dye adsorption decreases for higher concentrations of 0.26 mmol due to saturation of zeolite functional domains by acrylic acid. It can also be expressed that polymerization time has a little effect on dye removal. Therefore, we used concentrations of 0.17 and 0.26 mmol as the optimum concentrations for further studies.

3.6. Effect of initiator's concentration

Fig. 8 showed the effect of initiator content on dye adsorption of BR46 and BB41 by nanocomposites in single system. The dye adsorption increases as APS content increases, and decreases further by increasing the content of APS. The relation between the average kinetic chain length (υ) and concentration of the initiator in free-radical polymerization is given by the following equation [30]:

$$\upsilon = \frac{1}{2} k_p (f k_i k_t)^{-\frac{1}{2}} [I]^{-\frac{1}{2}} [M] \quad (5)$$

where k_p, k_i, and k_t are the rate constants for propagation, initiator, and termination, respectively; f is the efficiency of initiation by the initiator; and $[I]$ and $[M]$ are the initial concentration of the initiator and monomer, respectively. According to Eq. (4), the molecular weight in free-radical polymerization is decreased with an increase in initiator's concentration. With decreasing the molecular weight, the relative amount of polymer chain ends increases. As it was previously shown, the polymer chain end groups do not

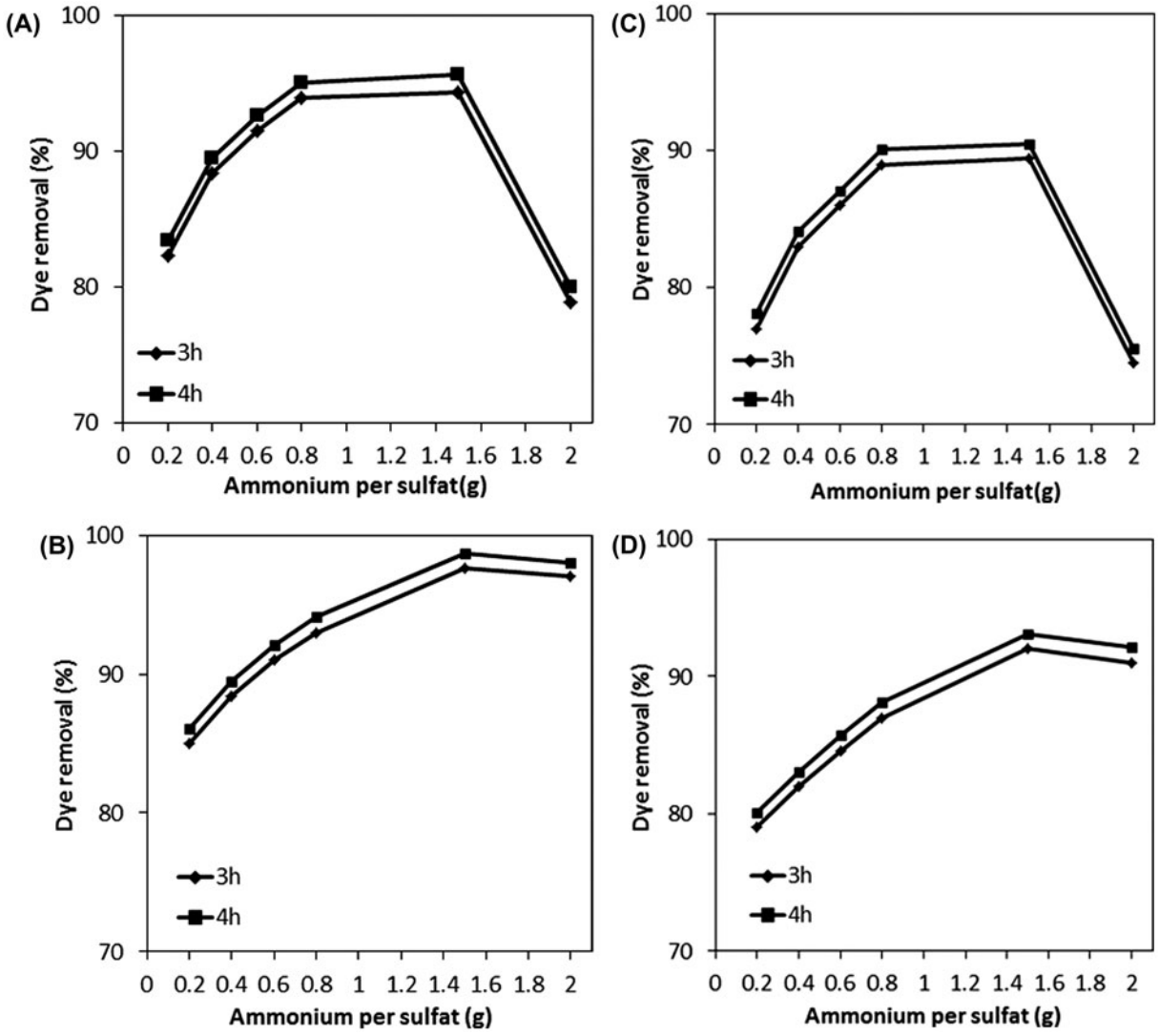

Fig. 8. The effect of initiator's concentration on dye adsorption of superabsorbent nanocomposites, (A) nanocomposite containing 0.17 mmol AA for BB41 dye, (B) nanocomposite containing 0.17 mmol AA for BR46 dye, (C) nanocomposite containing 0.26 mmol AA for BB41 dye, and (D) nanocomposite containing 0.26 mmolAA for BR46 dye.

contribute in the dye adsorption of nanocomposites [43]. Therefore, the increase in initiator content is responsible for decreasing the dye adsorption. However, further decreases in APS content below the optimum values are accompanied by a decrease in adsorbency of the prepared nanocomposite. This result may be attributed to a decrease in the number of radicals produced as the content of APS decreases. As the network cannot form efficiently with small number of radicals in the free-radical polymerization, this may result in the decrease in the dye adsorption. This is further confirmed by Pottier et al. [43].

According to Sections 3.3 and 3.4, it is obvious that there is negligible difference in dye removal ability of the synthesized composites with polymerization time of 3 and 4 h. Thus, we chose nanocomposites obtained by 0.26 mmol: AA/6.57 mmol: APS, 3 h and 0.17 mmol: AA/3.50 mmol: APS, 3 h as optimum adsorbents for further studies.

3.7. BR46 and BB41 adsorption time studies for zeolite and synthesized nanocomposites

Fig. 9 showed the effect of duration of dye removal of BR46 and BB41 from the solutions in single and binary systems. Various nanocomposites were prepared for comparing with untreated zeolite and we concluded that adsorption capacity of BR46 and BB41

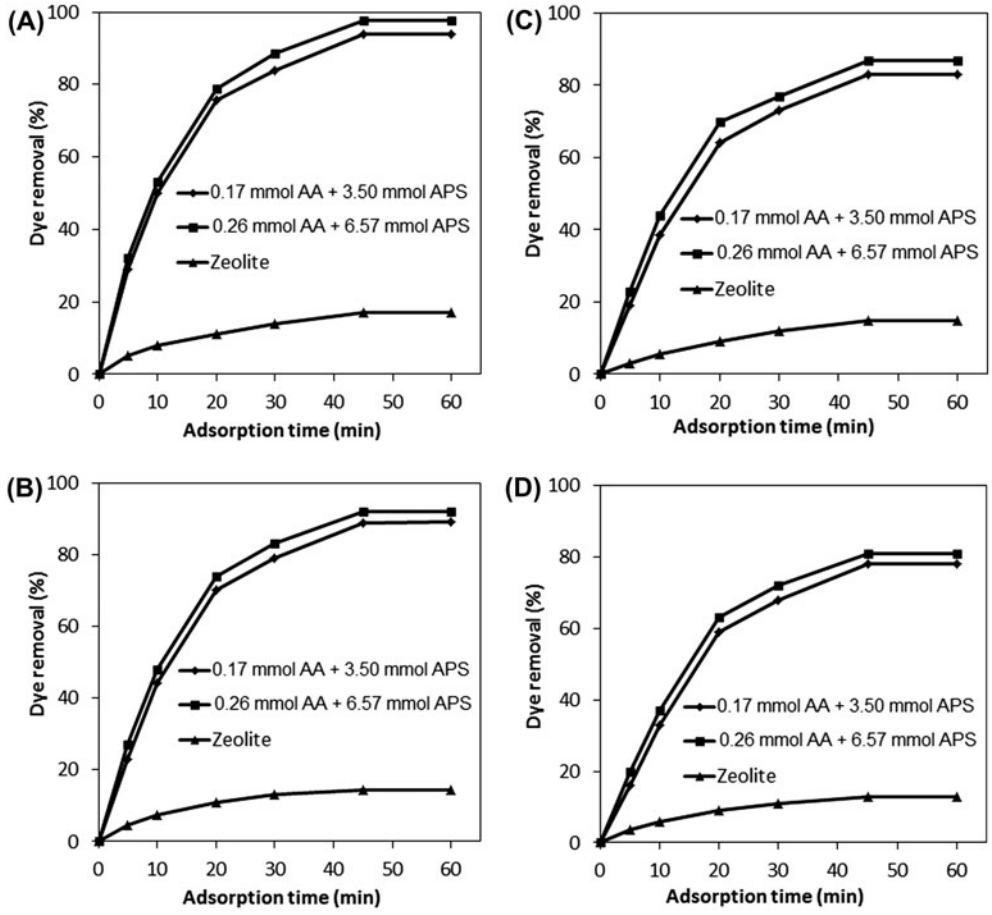

Fig. 9. The effect of duration of dye removal single and binary systems, (A) BB41 (sin), (B) BR46 (sin), (C) BB41 (bin), and (D) BR46 (bin).

increased about 82.4 and 83.35% for the nanocomposites with 0.17 mmol AA + 3.50 mmol APS and 0.26 mmol AA + 6.57 mmol: APS, respectively. With increasing the amount of AA in composites, the number of active sites (COOH) distributed on the surface of adsorbent increased, therefore the dye removal ability enhanced. It is evident from the equilibrium studies that equilibrium adsorption capacities decreased in the binary system (as compared to single dye system). Decreasing in the overall uptake capacity of the dyes in binary system is because of the presence of other dye due to the antagonistic interaction between dyes [44].

3.8. The effect of adsorbent dosage

The effect of adsorbent dosage on the removal of BR46 and BB41 in single and binary systems after one hour is given in Fig. 10. The possibility of interaction between nanocomposite particles and pollutants depends on the amount and type of adsorption sites in solution [44]. As can be seen, the adsorption process was initially rapid and then it slowed down, reached the equilibrium. Rapid adsorption of dyes at the initial minutes is due to a great number of vacant adsorption sites existing for interaction with dyes [45] and the high concentration of dye. Adsorption rate was after further treatment decreased because of saturation of the adsorptive sites as well as a decrease in the dye concentration.

With increasing the adsorbent dosage, the adsorption percent increases, but adsorption capacity decreases. An increase in adsorption percent can be attributed to more available adsorption sites at the nanocomposites surface; whereas the decrease in adsorption capacity is due to remain some of the adsorption sites unsaturated during the adsorption process.

According to Fig. 10, there was not considerable change in the removal of dyes for adsorbents with

0.005 and 0.007 g in single and binary systems; thus we considered 0.005 g of adsorbent as an optimal value for adsorption of both dyes in single and binary systems for further experiments.

3.9. Effect of initial dye concentration

Effect of initial dye concentration on removal of BR46 and BB41 in single and binary systems was studied and results are shown in Fig. 11. It can be seen that the dye removal percentage is decreased as the initial concentration of dye increased. Such a decrease is because of increasing the number of dye molecules against the constant adsorption sites of nanocomposites. It can be further stated that repulsion phenomenon occurs between adsorbed dye molecules on one hand and dye molecules in the aqueous solution on the other hand resulting to a decrease in removal percentage of dye from solution. The amount of the dye adsorbed onto the surface of composites increases with an increase in the initial dye concentration of solution. This can be due to an increase in the driving force of the concentration gradient at the higher initial dye concentration [46].

3.10. Effect of pH of solution on dye adsorption

The solution pH plays an important role in the adsorption behavior of nanocomposites. The pH of

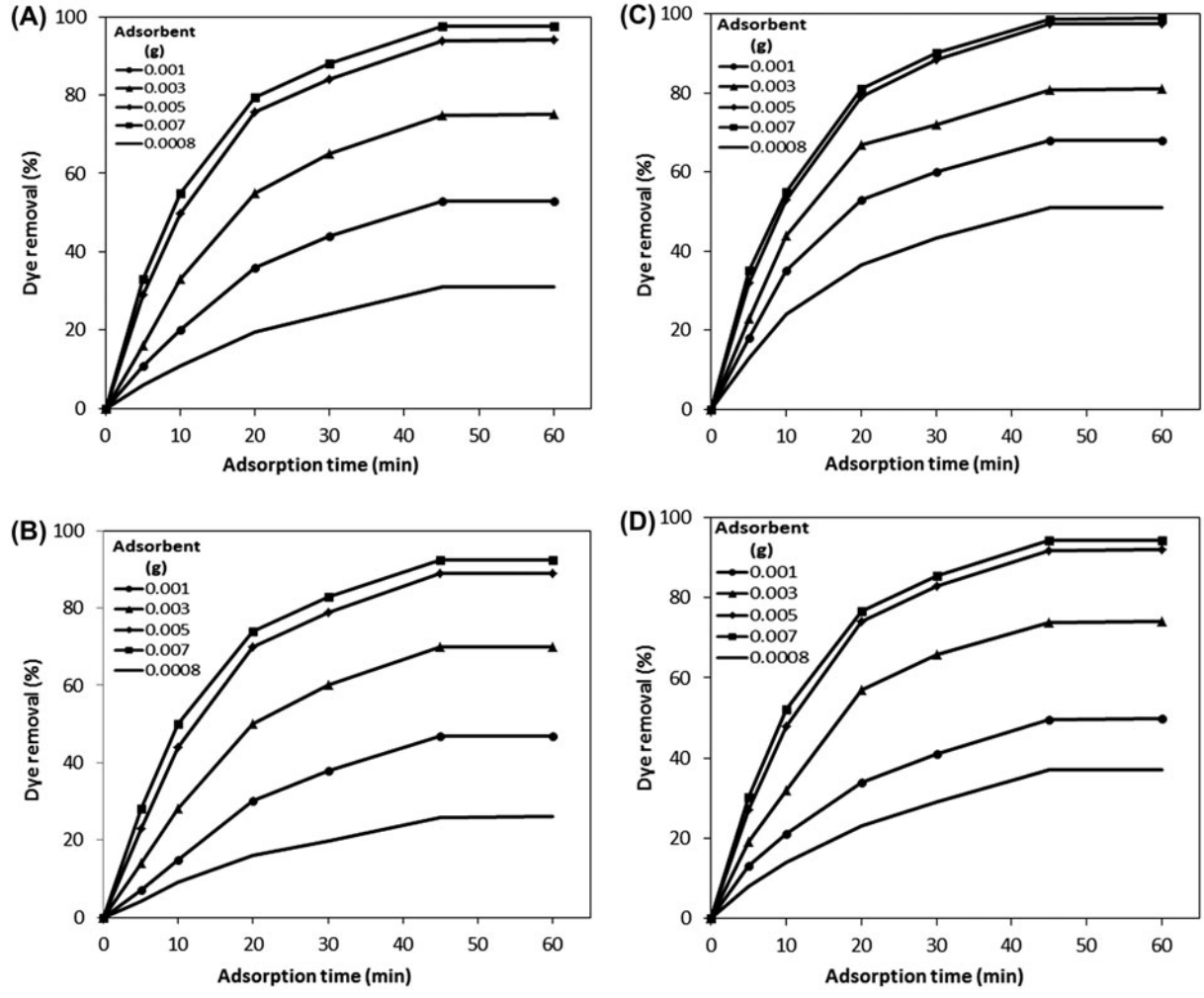

Fig. 10. Effect of adsorbents dosage on dye removal from single and binary systems by (A) zeolite treated with 0.14 mmol AA and 3.50 mmol APS for BB41 (sin), (B) zeolite treated with 0.17 mmol AA and 3.50 mmol APS for BR46 (sin), (C) zeolite treated with 0.26 mmol AA and 6.57 mmol APS for BB41 (sin), (D) zeolite treated with 0.26 mmol AA and 6.57 mmol APS for BR46 (sin), (E) zeolite treated with 0.17mmolL AA and 3.50 mmol APS for BB41 (bin), (F) zeolite treated with 0.17 mmol AA and 3.50 mmol APS for BR46 (bin), (G) zeolite treated with 0.26 mmol AA and 6.57 mmol APS for BB41 (bin), and (H) zeolite treated with 0.26 mmol AA and 6.57 mmol APS for BR46 (bin).

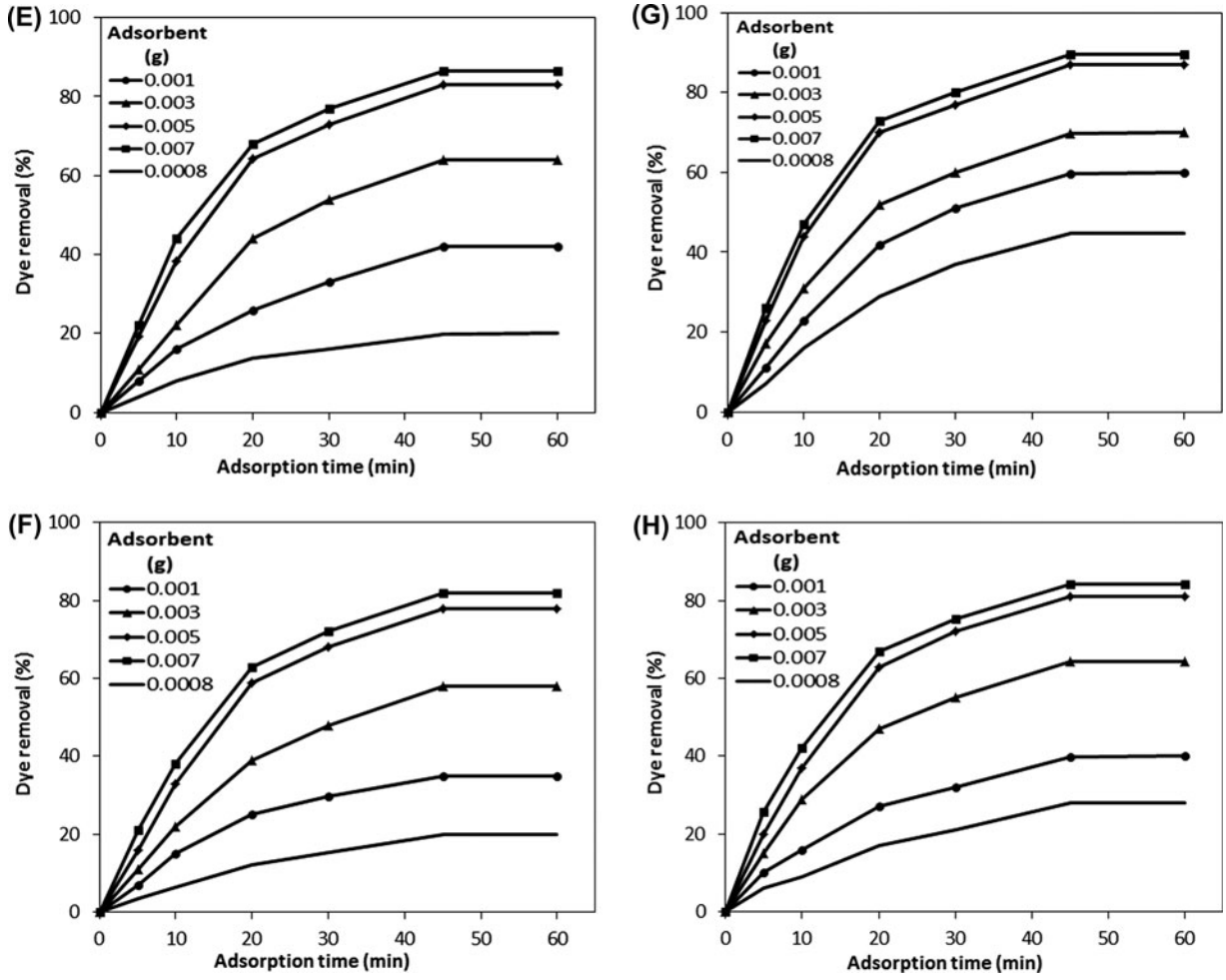

Fig. 10. (*Continued*).

solution affects the surface charge of adsorbent, degree of ionization of the dye in solution and separation of functional groups on the active sites of adsorbent and solution chemistry. Influence of solution pH on dye removal by nanocomposites in single and binary systems are shown in Fig. 12. As it can be seen in Figures (A)–(D), the adsorption efficiency at pH 6.8 is higher than other pHs. At low pH medium, removal percentage of dye is decreased due to the competition between H^+ ions and dye molecules in the solution. On the other hand, pH of alkaline behaves different in adsorption and dye molecules are possibly interacting with OH^-ions in solution resulting to decrease the dye affinity to nanocomposites.

3.11. Adsorption isotherms

Equilibrium relationships between sorbent and sorbet are described by sorption isotherms, which is the ratio between the quantity of sorbet and that remained in solution at a fixed temperature of equilibrium. In order to optimize the design of an adsorption system, it is important to establish the most appropriate correlation for the equilibrium curve [47]. In dye adsorption system, they present how the dye molecule can be distributed between the liquid and solid phases at various equilibrium concentrations and the relation between the mass of dye adsorbed per unit mass of adsorbent and liquid phase dye concentration at equilibrium.

Langmuir, Freundlich, and Temkin isotherms were used in this work. The Langmuir model that has been successfully applied to many adsorption processes [47–49] can be written as following equation:

$$q_e = \frac{Q_0 K_L C_e}{1 + K_L C_e} \quad (6)$$

where q_e is the amount of dye adsorbed on the nanocomposites at equilibrium, C_e is the equilibrium concentration of dye solution, K_L is the equilibrium constant, and Q_0 is the maximum adsorption capacity. Langmuir isotherm assumptions are: (i) adsorption takes place as a monolayer on the surface of adsorbent and the thickness of this layer is equal to one adsorbed molecule; (ii) adsorption can only occur at a finite number of localized sites that are identical and equivalent, with no interaction and steric hindrance between the adsorbed molecules or adjacent sites [50,51].

The linear form of Langmuir equation is:

$$\frac{C_e}{q_e} = \frac{1}{K_L Q_0} + \frac{C_e}{Q_0} \tag{7}$$

Isotherm data was also studied by the Freundlich isotherm, which can be expressed by following equation [52,53]:

$$q_e = K_F C_e^{\frac{1}{n}} \tag{8}$$

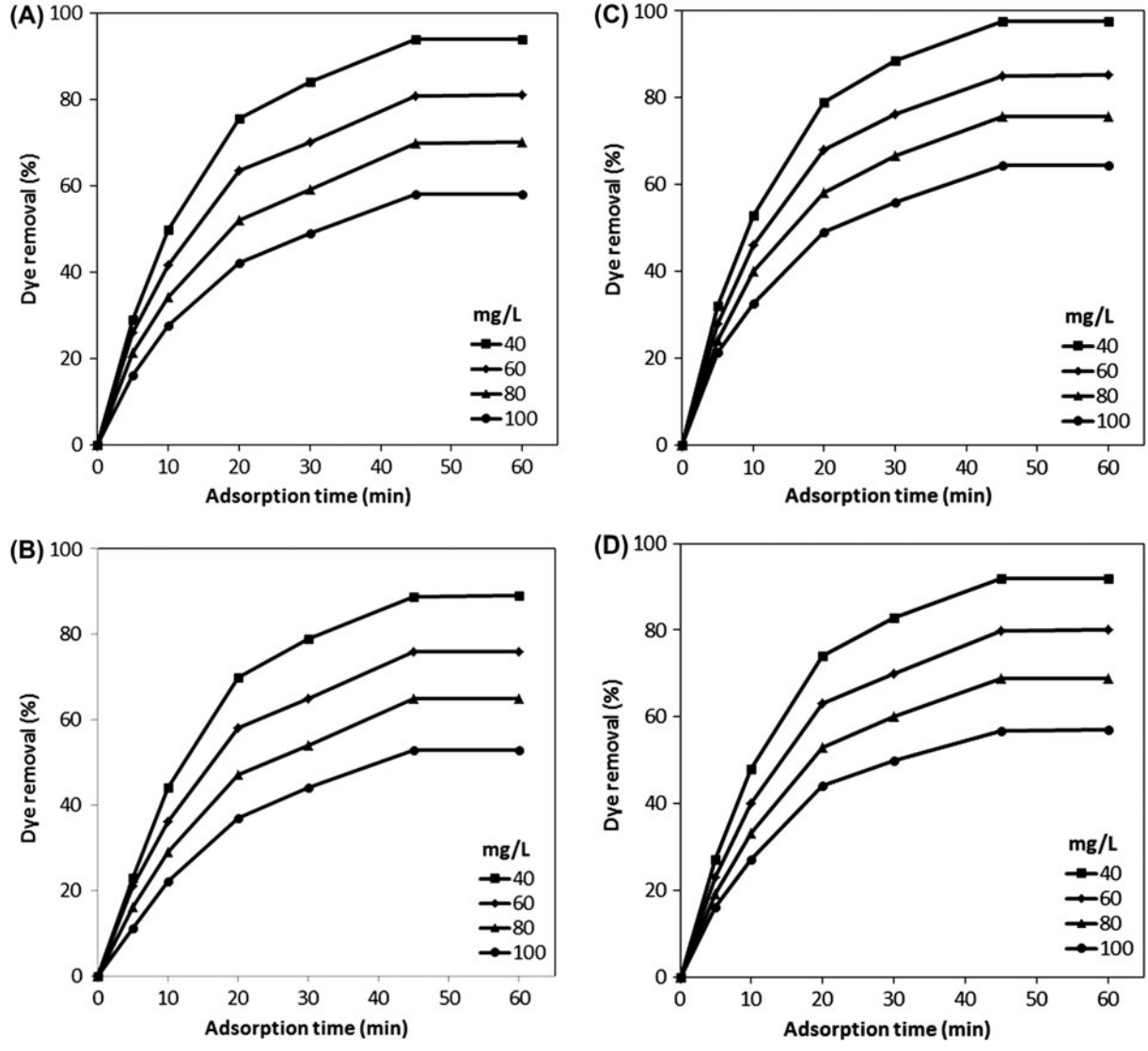

Fig. 11. Effect of initial dye concentration on dye removal from single and binary systems by (A) zeolite treated with 0.17 mmol AA and 3.50 mmol APS for BB41 (sin), (B) zeolite treated with 0.17 mmol AA and 3.50 mmol APS for BR46 (sin), (C) zeolite treated with 0.26 mmol AA and 6.57 mmol APS for BB41 (sin), (D) zeolite treated with 0.26 mmol AA and 6.57 mmol APS for BR46 (sin), (E) zeolite treated with 0.17 mmol AA and 3.50 mmol APS for BB41 (bin), (F) zeolite treated with 0.17 mmol AA and 3.50 mmol APS for BR46 (bin), (G) zeolite treated with 0.26mmolAA and 6.57 mmol APS for BB41 (bin), and (H) zeolite treated with 0.26 mmol AA and 6.57 mmol APS for BR46 (bin).

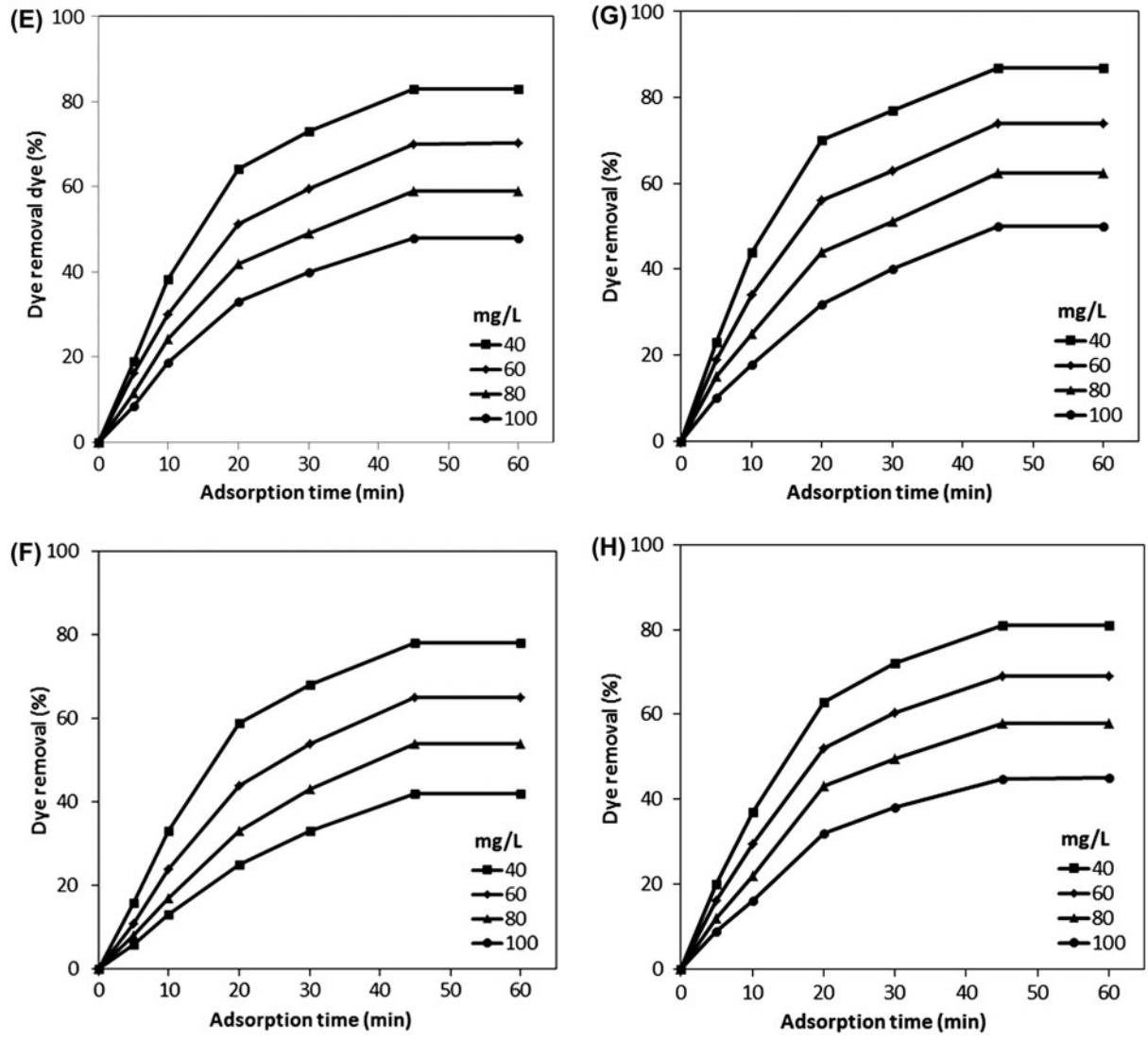

Fig. 11. (*Continued*).

where K_F is the adsorption capacity at unit concentration and is the adsorption intensity which ranges between 0 and 1 is a measure of adsorption intensity or surface heterogeneity, becoming more heterogeneous as its value gets closer to zero. Whereas, a value below unity implies chemisorptions process where above one is an indicative of cooperative adsorption. The basic assumption of this model is that there is an exponential variation in site energies of adsorbent, and also surface adsorption is not a rate-limiting step [54]. Eq. (8) can be rearranged to a linear form:

$$\log q_e = \log K_F + \frac{1}{n} \log C_e \tag{9}$$

The Temkin isotherm is given as:

$$q_e = \frac{RT}{b \ln(K_T C_e)} \tag{10}$$

Linearized form of Eq. (9) is written as:

$$q_e = B_1 \ln K_T + B_1 \ln C_e \tag{11}$$

where

$$B_1 = \frac{RT}{b} \tag{12}$$

K_T is the equilibrium binding constant (L/mol) corresponding to the maximum binding energy and constant B_1 is related to the heat of adsorption. T is also the absolute temperature (K), and R is the universal gas constant (8.314 J/mol/K).

The basic assumption of this isotherm is that heat of adsorption (function of temperature) of all molecules in the layer would decrease linearly rather than logarithmic with coverage [55]. As implied in the equation, its derivation is characterized by a uniform distribution of binding energies (up to some maximum binding energy).

In order to determine the constants in Langmuir, Freundlich, and Temkin isotherms, a plot of C_e/q_e vs. C_e, $\log q_e$ vs. $\log C_e$ and q_e vs. $\ln C_e$ were drawn, respectively. The coefficient values for isotherms are shown in Table 3.

R^2 value for Langmuir isotherm model showed that the dye removal isotherm for BR46 and BB41 in single and binary systems can be approximated as

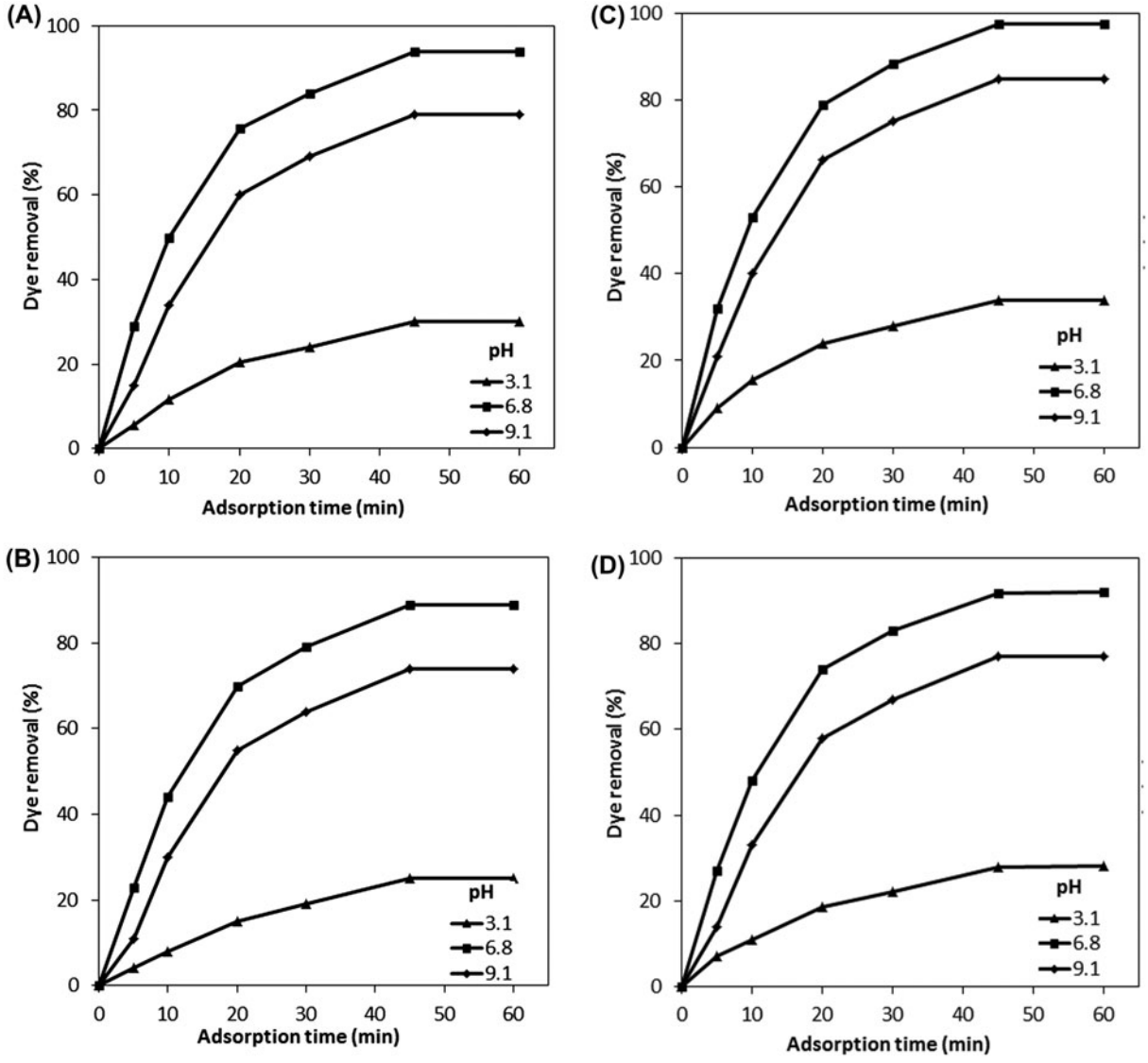

Fig. 12. Effect of pH of solution on dye removal from single and binary systems by (A) zeolite treated with 0.17 mmol AA and 3.50 mmol APS for BB41 (sin), (B) zeolite treated with 0.17 mmol AA and 3.50 mmol APS for BR46 (sin), (C) zeolite treated with 0.26 mmol AA and 6.57 mmol APS for BB41 (sin), (D) zeolite treated with 0.26 mmol AA and 6.57 mmol APS for BR46 (sin), (E) zeolite treated with 0.17 mmol AA and 3.50 mmol APS for BB41 (bin), (F) zeolite treated with 0.17 mmol AA and 3.50 mmol APS for BR46 (bin), (G) zeolite treated with 0.26 mmol AA and 6.57 mmol APS for BB41 (bin), and (H) zeolite treated with 0.26 mmol AA and 6.57 mmol APS for BR46 (bin).

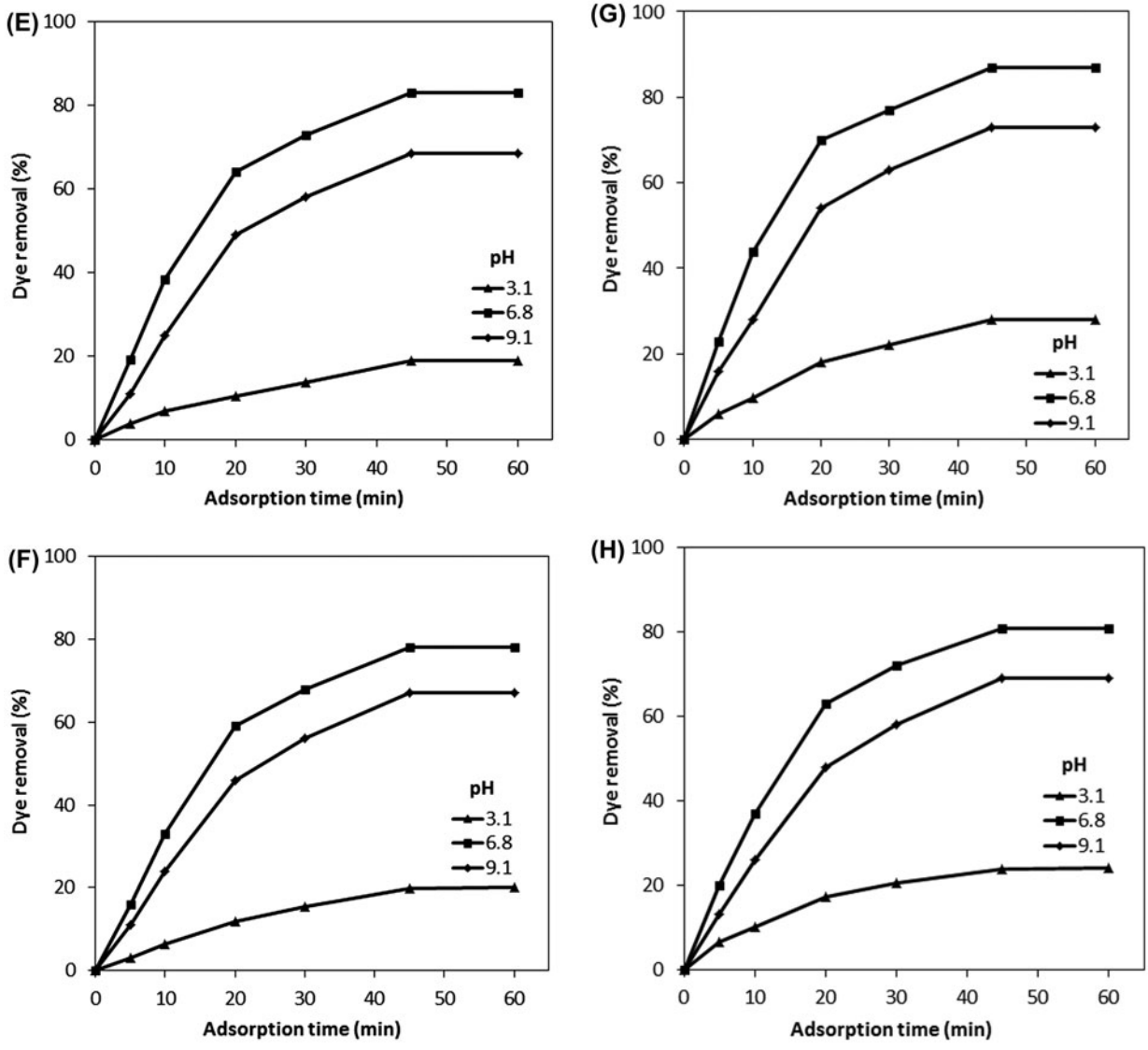

Fig. 12. (*Continued*).

Langmuir model. This means that the adsorption of the dyes takes place at specific homogeneous sites by functional domains of nanocomposites.

3.12. Adsorption kinetics

Adsorption kinetics provided information regarding the mechanisms of adsorption that are important for the efficiency of the process. In order to design an effective model, investigation was made on the adsorption rate. Several kinetics models (pseudo-first-order, pseudo-second-order, and intraparticle diffusion) are used to test the experimental data such as the examination of the controlling mechanism of the adsorption process [56,57]. A linear form of pseudo-first-order model was described by Lagergren as following equation:

$$\mathrm{d}q_t/\mathrm{d}t = K_1(q_\mathrm{e} - q_t) \tag{13}$$

where q_e is the amount of dye adsorbed at equilibrium (mg/g), q_t is the amount of dye adsorbed at t time (mg/g) and K_1 is the equilibrium rate constant of pseudo-first-order adsorption (min^{-1}).

The pseudo-second-order adsorption model, in its final form, can be expressed as follows [58]:

$$\log(q_\mathrm{e} - q_t) = \log(q_\mathrm{e}) - \frac{K_1}{2.303}t \tag{14}$$

Table 3
Correlation coefficient for adsorption isotherms on zeolite/AA nanocomposites

		Langmuir			Freundlich				Temkin	
Adsorbent	Dye	R^2	Q_0 (mg/g)	K_L	R^2	$1/n$	K_F	R^2	B_1	K_T (L/mol)
0.17 mmol AA + 3.50 mmol APS	*Single*									
	BB41	0.998	2,439.02	0.488	0.897	0.157	1,318.25	0.909	295.91	68.03
	BR46	0.999	2,272.72	0.354	0.901	0.176	1,114.29	0.894	308.99	24.28
	Binary (BB41 + BR46)									
	BB41	0.999	2,083.33	0.263	0.882	0.169	933.25	0.904	304.13	12.67
	BR46	0.996	1,785.71	0.314	0.870	0.188	891.25	0.874	248.58	20.69
0.26 mmol AA + 6.57 mmol APS	*Single*									
	BB41	0.996	2,702.70	0.596	0.910	0.146	1,513.56	0.927	291.26	181.86
	BR46	0.999	2,380.95	0.415	0.917	0.175	1,218.98	0.915	323.9	30.56
	Binary (BB41 + BR46)									
	BB41	0.999	2,127.65	0.376	0.887	0.169	1,071.51	0.906	285.75	28.30
	BR46	0.996	1,923.07	0.335	0.864	0.172	939.72	0.869	275.87	17.46

where q_e is the amount of dye adsorbed at equilibrium (mg/g), q_t is the amount of dye adsorbed at t time (mg/g), and K_1 is the equilibrium rate constant of pseudo-first-order adsorption (min^{-1}).

The pseudo-second-order adsorption model, in its final form, can be expressed as follows [58]:

$$\frac{t}{q_t} = \frac{1}{Kq_e^2} + \frac{1}{q_e}t \tag{15}$$

The possibility of intraparticle diffusion resistance affecting adsorption is explored using the intraparticle diffusion model as:

$$q_t = k_p t^{\frac{1}{2}} + I \tag{16}$$

where k_p and I are the intraparticle diffusion rate constant and intercept, respectively. Values of I give an idea about the thickness of the boundary layer, i.e. the larger intercept the greater is the boundary layer effect [59]. To understand the applicability of the intraparticle diffusion, pseudo-second-order and pseudo-first-order, linear plots of q_t against $t^{1/2}$, t/q_t vs. t and log $(q_e - q_t)$ vs. t at different dye concentrations [(40, 60, 80, and 100) mg/L] are plotted, respectively. The kinetic constants for dye adsorption are shown in Table 4 as supplementary data.

Results illustrated that the rates of sorption conform to the pseudo-second-order kinetic model with good coefficients of determination. In addition, the experimental q_e ($(q_e)_{Exp.}$) values consistent with the calculated ones ($(q_e)_{Cal.}$), obtained from the linear plots of pseudo-second-order kinetics.

Such a result confirming that the chemical adsorption of dye into the adsorbent is more than the physical one [60,61].

4. Conclusion

In this research, zeolite–acrylic acid nanocomposite was synthesized as a function of the monomer and catalyst concentration as well as duration of process. Prepared nanocomposites were further considered for the removal of BR46 and BB41 dyes in single and binary systems. Incorporation of acrylic acid on the zeolite can improve significantly the adsorption capacity of composites and adsorption had highest efficiency at pH 6.8. Results illustrated that the overall uptake capacity of the dyes in binary system decreased because of the presence of other dye due to the antagonistic interaction between dyes. The experimental results were analyzed using the Langmuir, Freundlich, and Temkin models and the correlation coefficient of model in single and binary systems are fitted to Langmuir equation. The data indicated that the adsorption kinetics of dyes on the composites in single and binary systems follow the pseudo-second-order rate expression. This study demonstrates that zeolite–acrylic acid nanocomposite is a useful material for the removal of basic dyes from effluents.

Supplementary material

The supplementary material for this paper is available online at http://dx.doi.10.1080/19443994.2015.1112841.

References

[1] D. Şolpan, S. Duran, D. Saraydin, O. Güven, Adsorption of methyl violet in aqueous solutions by poly (acrylamide-co-acrylic acid) hydrogels, Radiat. Phys. Chem. 66 (2003) 117–127.

[2] L.M. Zhang, Y.J. Zhou, Y. Wang, Novel hydrogel composite for the removal of water-soluble cationic dye, J. Chem. Technol. Biotechnol. 81 (2006) 799–804.

[3] Y. Xu, R.E. Lebrun, P.-J. Gallo, P. Blond, Treatment of textile dye plant effluent by nanofiltration membrane, Sep. Sci. Technol. 34 (1999) 2501–2519.

[4] T. Bechtold, E. Burtscher, A. Turcanu, Cathodic decolourisation of textile waste water containing reactive dyes using a multi-cathode electrolyser, J. Chem. Technol. Biotechnol. 76 (2001) 303–311.

[5] N. Akhtar, J. Iqbal, M. Iqbal, Enhancement of lead(II) biosorption by microalgal biomass immobilized onto Loofa (*Luffa cylindrica*) sponge, Eng. Life Sci. 4 (2004) 171–178.

[6] L.V. Gonzalez-Gutierrez, E.M. Escamilla-Silva, Reactive red azo dye degradation in a UASB bioreactor: Mechanism and kinetics, Eng. Life Sci. 9 (2009) 311–316.

[7] N. Kannan, M.M. Sundaram, Kinetics and mechanism of removal of methylene blue by adsorption on various carbons—A comparative study, Dyes Pigm. 51 (2001) 25–40.

[8] Y.M. Slokar, A.M.L. Marechal, Methods of decoloration of textile wastewaters, Dyes Pigm. 37 (1998) 335–356.

[9] P. Cooper, Removing colour from dyehouse waste waters—A critical review of technology available, J. Soc. Dyers Colour. 109 (1993) 97–100.

[10] V. Meshko, L. Markovska, M. Mincheva, A.E. Rodrigues, Adsorption of basic dyes on granular acivated carbon and natural zeolite, Water Res. 35 (2001) 3357–3366.

[11] S. Sadaf, H.N. Bhatti, Batch and fixed bed column studies for the removal of Indosol Yellow BG dye by peanut husk, J. Taiwan Inst. Chem. Eng. 45 (2014) 541–553.

[12] S. Sadaf, H.N. Bhatti, S. Nausheen, S. Noreen, Potential use of low-cost lignocellulosic waste for the Removal of Direct Violet 51 from Aqueous Solution: Equilibrium and breakthrough studies, Arch. Environ. Contam. Toxicol. 66 (2014) 557–571.

[13] S. Nawaz, H.N. Bhatti, T.H. Bokhari, S. Sadaf, Removal of Novacron Golden Yellow dye from aqueous solutions by low-cost agricultural waste: Batch and fixed bed study, Chem. Ecol. 30 (2013) 52–65.

[14] S. Noreen, H.N. Bhatti, S. Nausheen, S. Sadaf, M. Ashfaq, Batch and fixed bed adsorption study for the removal of Drimarine Black CL-B dye from aqueous solution using a lignocellulosic waste: A cost affective adsorbent, Ind. Crops Prod. 50 (2013) 568–579.

[15] S. Sadaf, H.N. Bhatti, Evaluation of peanut husk as a novel, low cost biosorbent for the removal of Indosol Orange RSN dye from aqueous solutions: Batch and fixed bed studies, Clean Technol. Environ. Policy 16 (2013) 527–544.

[16] M.A. Mohd Salleh, D. Khalid Mahmoud, W. Azlina Wan Abdul Karim, A. Idris, Cationic and anionic dye adsorption by agricultural solid wastes: A comprehensive review, Desalination 280 (2011) 1–13.

[17] M. Inyang, B. Gao, Y. Yao, Y. Xue, A.R. Zimmerman, P. Pullammanappallil, X. Cao, Removal of heavy metals from aqueous solution by biochars derived from anaerobically digested biomass, Bioresour. Technol. 110 (2012) 50–56.

[18] F. Bouhamed, Z. Elouear, J. Bouzid, B. Ouddane, Multi-component adsorption of copper, nickel and zinc from aqueous solutions onto activated carbon prepared from date stones, Environ. Sci. Pollut. Res. First online: 07 April (2015) 1–6. Available from: <http://link.springer.com/article/10.1007%2Fs11356-015-4400-3>.

[19] S.R. Khairkar, A.R. Raut, Chitosan-graft-poly(acrylicacid-co-acrylamide) superabsorbent hydrogel, J. Chitin Chitosan Sci. 2 (2014) 288–292.

[20] F. Libau, Structural Chemistry of Silicates: Structure, Bonding, and Classification, Springer-Verlag, Berlin, 2012.

[21] C. Baerlocher, L.B. McCusker, D.H. Olsan, Atlas of Zeolite Framework Types, sixth ed., Elsevier, Amsterdam, The Netherlands, 2007.

[22] D.W. Breck, Zeolite Molecular Sieves, Wiley, New York, NY, 1974.

[23] D.A. Faux, W. Smith, T.R. Forester, Molecular dynamics studies of hydrated and dehydrated Na^+-zeolite-4A, J. Phys. Chem. B 101 (1997) 1762–1768.

[24] L. Qiu, Thermal Properties of Framework Materials: Selected Zeolites, Clathrates and an Organic Diol, PhD thesis, 2000. Available from: <http://www.collectionscanada.gc.ca/obj/s4/f2/dsk1/tape3/PQDD_0035/NQ66643.pdf>.

[25] D.N. Huyen, N.T. Tung, N.D. Thien, L.H. Thanh, Effect of TiO_2 on the gas sensing features of TiO_2/PANi nanocomposites, Sensors 11 (2011) 1924–1931.

[26] W. Jihuai, L. Jianming, Zh. Meng, W. Congrong, Synthesis and properties of starch-*graft*-polyacrylamide/clay superabsorbent composite, Macromol. Rapid Commun. 21 (2000) 1032–1034.

[27] L. Jianming, W. Jihuai, Y. Zheng Fang, P. Minli, Synthesis and properties of poly(acrylic acid)/mica superabsorbent nanocomposite, Macromol. Rapid Commun. 22 (2001) 422–424.

[28] W. Lee, Y. Chen, Effect of intercalated reactive mica on water absorbency for poly(sodium acrylate) composite superabsorbents, Eur. Polym. J. 41 (2005) 1605–1612.

[29] S.R. Shirsath, A.P. Patil, R. Patil, J.B. Naik, P.R. Gogate, S.H. Sonawane, Removal of Brilliant Green from wastewater using conventional and ultrasonically prepared poly(acrylic acid) hydrogel loaded with kaolin clay: A comparative study, Ultrason. Sonochem. 20 (2013) 914–923.

[30] Z. Xiuju, Z. Shaojie, Z. lin, Z. Jingjing, Removal of basic Fuchsin dye by adsorption onto polyacrylamide/laponite nanocomposite hydrogels, Metal-Org. Nano-Met. Chem. 42 (2012) 1273–1277.

[31] Y. Wang, L. Zeng, X. Ren, H. Song, A. Wang, Removal of Methyl Violet from aqueous solutions using poly (acrylic acid-*co*-acrylamide)/attapulgite composite, J. Environ. Sci. 22 (2010) 7–14.

[32] M. Parvinzadeh Gashti, A. Almasian, UV radiation induced flame retardant cellulose fiber by using polyvinylphosphonic acid/carbon nanotube composite coating, Compos. Part B 45 (2012) 282–489.

[33] M. Parvinzadeh, S. Eslami, Optical and electromagnetic characteristics of clay–iron oxide nanocomposites, Res. Chem. Intermed. 37 (2011) 771–784.
[34] M. Parvinzadeh Gashti, S. Eslami, Structural, optical and electromagnetic properties of aluminum–clay nanocomposites, Superlattices Microstruct.. 51 (2012) 135–148.
[35] K.H. Keith Choy, F.J. Porter, M. Gordon, Langmuir isotherm models applied to the multicomponent sorption of acid dyes from effluent onto activated carbon, J. Chem. Eng. Data 45 (2000) 575–584.
[36] R. Hajiraissi, M. Parvinzadeh, Preparation of polybutylene terephthalate/silica nanocomposites by melt compounding: Evaluation of surface properties, Appl. Surf. Sci. 257 (2011) 8443–8450. Available from: <http://www.sciencedirect.com/science/journal/01694332/257/20>.
[37] Y.S. Ho, G. McKay, Pseudo-second order model for sorption processes, Process Biochem. 34 (1999) 451–465.
[38] M. Parvinzadeh, S. Moradian, A. Rashidi, M.E. Yazdanshenas, Effect of the addition of modified nanoclays on the surface properties of the resultant polyethylene terephthalate/clay nanocomposites, Polym.-Plast. Technol. Eng. 49 (2010) 874–884.
[39] M. Parvinzadeh, I. Ebrahimi, Influence of atmospheric-air plasma on the coating of a nonionic lubricating agent on polyester fiber, Radiat. Eff. Defects Solids 166 (2011) 408–416.
[40] Z. Tang, Q. Liu, Q. Tang, J. Wu, J. Wang, S. Chen, C. Cheng, H. Yu, Z. Lan, J. Lin, M. Huang, Preparation of PAA-g-CTAB/PANI polymer based gel-electrolyte and the application in quasi-solid-state dye-sensitized solar cells, Electrochim. Acta 58 (2011) 52–57.
[41] M. Parvinzadeh Gashti, A. Almasian, Synthesizing tertiary silver/silica/kaolinite nanocomposite using photo-reduction method: Characterization of morphology and electromagnetic properties, Composites Part B 43 (2012) 3374–3383.
[42] Z. Huang, X. Yang, X. Pan, Y. Zhao, M. Feng, Q. Zhao, Thermal degradation study of sodium alginate-zeolite 4A composites, Proceedings of the 17th IAPRI World Conference on Packaging, Tianjin, China, 2010.
[43] A.S. Pottier, S. Cassaignon, C. Chanéac, F. Villain, E. Tronc, J.P. Jolivet, Size tailoring of TiO_2 anatase nanoparticles in aqueous medium and synthesis of nanocomposites. Characterization by Raman spectroscopy, J. Mater. Chem. 13 (2003) 877–882.
[44] Z.S. Liu, G.L. Rempel, Preparation of superabsorbent polymers by crosslinking acrylic acid and acrylamide copolymers, J. Appl. Polym. Sci. 64 (1997) 1345–1353.
[45] M. Turabik, Adsorption of basic dyes from single and binary component systems onto bentonite: Simultaneous analysis of Basic Red 46 and Basic Yellow 28 by first order derivative spectrophotometric analysis method, J. Hazard. Mater. 158 (2008) 52–64.
[46] E.T. Kang, K.G. Neoh, K.L. Tan, Polyaniline: A polymer with many interesting intrinsic redox states, Prog. Polym. Sci. 23 (1998) 277–324.
[47] N.M. Mahmoodi, B. Hayati, M. Arami, F. Mazaheri, Single and binary system dye removal from colored textile wastewater by a dendrimer as a polymeric nanoarchitecture: Equilibrium and kinetics, J. Chem. Eng. Data 55 (2010) 4660–4668.
[48] N.M. Mahmoodi, F. Najafi, Synthesis, amine functionalization and dye removal ability of titania/silica nano-hybrid, Microporous Mesoporous Mater. 156 (2012) 153–160.
[49] A. Kurniawan, H. Sutiono, N. Indraswati, S. Ismadji, Removal of basic dyes in binary system by adsorption using rarasaponin–bentonite: Revisited of extended Langmuir model, Chem. Eng. J. 189–190 (2012) 264–274.
[50] R. Salehi, M. Arami, N.M. Mahmoodi, H. Bahrami, Sh. Khorramfar, Novel biocompatible composite (Chitosan–zinc oxide nanoparticle): Preparation, characterization and dye adsorption properties, Colloids Surf., B 80 (2010) 86–93.
[51] K. Balapure, N. Bhatt, D. Madamwar, Mineralization of reactive azo dyes present in simulated textile waste water using down flow microaerophilic fixed film bioreactor, Bioresour. Technol. 175 (2015) 1–7.
[52] N.M. Mahmoodi, F. Najafi, A. Neshat, Poly (amidoamine-co-acrylic acid) copolymer: Synthesis, characterization and dye removal ability, Ind. Crops Prod. 42 (2013) 119–125.
[53] E. Malkoc, Y. Nuhoglu, M. Dundar, Adsorption of chromium(VI) on pomace—An olive oil industry waste: Batch and column studies, J. Hazard. Mater. 138 (2006) 142–151.
[54] H.M.F. Freundlich, Over the adsorption in solution, J. Phys. Chem. 57 (1906) 385–470.
[55] A.W. Adamson, A.P. Gast, Physical Chemistry of Surfaces, sixth ed., Wiley-Interscience, New York, NY, 1967.
[56] J. Zeldowitsch, Adsorption site energy distribution, Acta Phys. Chim. 1 (1934) 961–973.
[57] C. Aharoni, M. Ungarish, Kinetics of activated chemisorption. Part 2—Theoretical models, J. Chem. Soc. Faraday Trans. 73 (1977) 456–464.
[58] Y.S. Ho, Citation review of Lagergren kinetic rate equation on adsorption reactions, Scientometrics 59 (2003) 171–177.
[59] Y.S. Ho, C.C. Chiang, Sorption studies of acid dye by mixed sorbents, Adsorption 7 (2001) 139–147.
[60] M. Monier, D.M. Ayad, A.A. Sarhan, Adsorption of Cu(II), Hg(II), and Ni(II) ions by modified natural wool chelating fibers, J. Hazard. Mater. 176 (2009) 348–355.
[61] S. Senthilkumaar, P. Kalaamani, K. Porkodi, P.R. Varadarajan, C.V. Subburaam, Adsorption of dissolved Reactive red dye from aqueous phase onto activated carbon prepared from agricultural waste, Bioresour. Technol. 97 (2006) 1618–1625.